RESEARCH PAPER

Consolidation and swelling behavior of kaolinite clay containing xanthan gum biopolymer

Yeong-Man Kwon[1,3] · Ilhan Chang[2] · Gye-Chun Cho[1]

Abstract

Recently, microbial biopolymer-based soil treatment (BPST) has gained attention for its application in environmentally friendly soil stabilization, particularly for enhancing the strength and stability of fine-grained soils. However, the effects of BPST on clay's compressibility (consolidation) and expansion (swelling) behaviors remain unclear. This study used xanthan gum, a microbially produced polysaccharide with anionic charges, to stabilize kaolinite clay. The effect of xanthan gum BPST on the consolidation and swelling behavior of cohesive kaolinite clays was assessed through a series of experimental tests, including one-dimensional consolidation tests with elastic wave measurements, swelling tests, environmental scanning electron microscopy, and unconsolidated-undrained triaxial tests. The formation of xanthan gum hydrogels induces pore-clogging, resulting in a delay in the consolidation process, increased energy dissipation, and compressibility. Furthermore, the interaction between kaolinite and xanthan gum improved the undrained shear strength of kaolinite soils, thereby reducing the consolidation time required for a specific bearing capacity. This study demonstrates the possible application of controlling hydraulic conductivity, seismic stabilization, and rapid surface stabilization. However, additional drainage is necessary for in situ applications.

Abbreviations

XG	Xanthan gum
m_b	Weight of biopolymer (g)
m_w	Weight of pore fluid (g)
m_s	Weight of kaolinite (g)
m_b/m_s	The xanthan gum-to-soil ratio in mass (%)
DI	Deionized water
e_i	Initial void ratio
e_p	Void ratio at the end of primary consolidation
c_v	Coefficient of consolidation (cm^2/s)
k	Permeability (cm/s)
$c_{\alpha e}$	The coefficient of secondary consolidation (cm^2/s)
C_c	Compression index
C_S	Swelling index
V_P	P-wave velocity (m/s)
V_S	S-wave velocity (m/s)

✉ Ilhan Chang
  ilhanchang@ajou.ac.kr

✉ Gye-Chun Cho
  gyechun@kaist.edu

  Yeong-Man Kwon
  yeongman.kwon@northwestern.edu

1   Department of Civil and Environmental Engineering, Korea Advanced Institute of Science and Technology (KAIST), Daejeon 34141, Republic of Korea

2   Department of Civil Systems Engineering, Ajou University, Suwon-Si 16499, Republic of Korea

3   Department of Civil and Environmental Engineering, Northwestern University, 2145 Sheridan Road, Evanston, Illinois 60208, USA

1 Introduction

Ground improvement is an essential civil engineering practice to enhance the stability of civil infrastructure by increasing soil strength and stiffness, improving erosion resistance, and controlling hydraulic conductivity [42]. In antiquity, ground improvement practices commonly used bio-based organic materials such as animal blood, dung, tree pods, straw, plant stems, and leaves [40]. However, artificial chemical stabilizer (e.g., Portland cement) has become the predominant ground improvement material

since the industrial revolution because of properties such as strengthening effectiveness and the high socioeconomic demand for rapid development [62, 96]. However, chemical ground improvement materials, such as cement, lime, and fly ash, have several environmental concerns, including massive carbon dioxide emissions, toxic substances, and an increase in the pH of the surrounding soil and underground water [24, 58]. Therefore, bio-mediated geomaterials are gaining popularity as environmentally friendly soil treatment and ground improvement binders for sustainable development. Biopolymer-based soil treatment (BPST) is being actively studied as a new approach nowadays [11, 14, 29, 37, 49, 90, 94, 97, 98].

Biopolymers are high-molecular-weight polysaccharides derived from natural sources, including cellulose, proteins (e.g., gelatin, casein, and silk), metabolic by-products of microorganisms (e.g., xanthan gum, gellan gum), and plant products such as guar gum and starch [29]. Previous research has demonstrated that BPST is an effective soil stabilization and ground improvement method in terms of strength enhancement [26, 30, 54, 71], soil hydraulic erosion control [48, 68, 69, 87], aeolian dust mitigation [32], and ground hydraulic conductivity reduction [18, 99]. Furthermore, BPST has advantages over other environment-friendly soil stabilization methods for use in fine-grained soils, consistent quality control, and a stable gel matrix [35].

A majority of the previous studies on the BPST focused on their application for cohesionless soils such as sand, silts, and mine tailings [1, 13, 18, 25, 33, 43, 61, 76]. However, biopolymers electrostatically interact with charged cohesive soils, increasing the liquid limits, shear strength, and promoting clay particle aggregation, which facilitates sedimentation [28, 67, 85]. Because of factors such as low bearing capacity, differential settlement, and lateral movements in fine-grained soils with low shear strength and high compressibility [50, 72, 88], soft cohesive soils should be improved to increase shear strength and control compressibility before construction [78]. Several techniques, including replacement, densification, hydraulic modification, chemical stabilization, and electrical modifications, have been employed to enhance the hydraulic and mechanical properties of soft soils [44, 52, 53, 75]. Among these, the biopolymer was employed in this study because this method is an eco-friendly approach for chemical stabilization for soft cohesive soils.

Previous research [71, 84, 111, 112] analyzed the effect of biopolymers on soft soil stabilization in terms of consolidation, which is a crucial factor to consider when evaluating the potential benefits of BPST. However, the consolidation behavior of fine-grained soils for the biopolymer method is complex and variable. For instance,

Latifi et al. [71] stated that biopolymer treatment (1% of soil mass) reduced the compression index (C_c) values of fine-grained soils (bentonite and kaolinite) due to the formation of hydrostatic and electrostatic bonds between kaolinite and biopolymer monomers. Other studies have also reported a decrease in collapsible potential [10, 36] and compressibility [100] with biopolymer treatment. Nugent et al. [84] demonstrated that anionic biopolymers increase the compressibility of kaolinite (initial void ratio of 2–2.7) by dissipating repulsive forces between anionic biopolymer strands and kaolinite particles under high vertical loads. Another consolidation analysis of biopolymer-treated cohesive soils [17, 97] also reported an increase in compressibility. These contrasting mechanisms of BPST on clay compressibility may be attributable to the complex interaction between the biopolymer and clays that varied according to the soil properties (e.g., mineral type, initial void ratio) and pore fluid characteristics (i.e., biopolymer type, ionic strength, and gel rheology) [107, 108]. Further, several studies have reported changes in the consolidation parameters (e.g., compressibility, coefficient of consolidation) according to the biopolymers, and a few studies have examined changes in the mechanical properties (e.g., mechanical wave, undrained shear strength) during the consolidation process. Consequently, it is necessary to analyze the alteration in fabrics [77] and mechanical waves [41] that are caused by the biopolymer during the consolidation process.

This study, therefore, assessed the effect of xanthan gum biopolymer (XG) on the consolidation of kaolinite clay with a high water content based on the microscale interaction between kaolinite clay, pore water, and XG biopolymer through consolidation and swelling stages. At constant vertical confinement of 5 kPa, the swelling pressure of XG-treated kaolinite was determined via a swelling test. A series of one-dimensional (1-D) consolidation tests were conducted on the untreated and XG-treated kaolinite specimens. The elastic wave (i.e., P-wave and S-wave) velocity of the clays was measured during the consolidation stages to obtain effective stress, energy dissipation, and small-strain stiffness variations. The possible interactions and structures between XG and kaolinite in the presence of water were analyzed using environmental scanning electron microscopy (ESEM) images. Lastly, unconsolidated-undrained (UU) triaxial tests were conducted to estimate the variation in undrained shear strength during consolidation, which is crucial for the surface stabilization of soft soils. This study demonstrates the consolidation and swelling behavior of XG-treated kaolinite, along with the changes in the material's mechanical properties during consolidation, and expands upon the foundation of BPST to improve cohesive soils.

2 Materials and methods

2.1 Materials

2.1.1 Fine soil: kaolinite

This study used Bintang kaolinite (Belitung Island, Indonesia). The unified soil classification system (USCS) classifies Bintang kaolinite as highly plastic clay (CH) with a plastic limit of 24% and a liquid limit of 70% [6]. The average specific surface area was 22 m^2/g, obtained through the methylene blue adsorption method [93]. The particle size distribution (Fig. 1a) of kaolinite was determined using a laser diffraction particle size analyzer (HELOS/KR-H2487) based on the ASTM International D4464-15 and B822-20 standards [3, 8]. The SEM image of kaolinite (Fig. 1b) revealed that the dominant morphology of the kaolinite used was a plate, whereas lath kaolinite was also present. Before the experiments, the
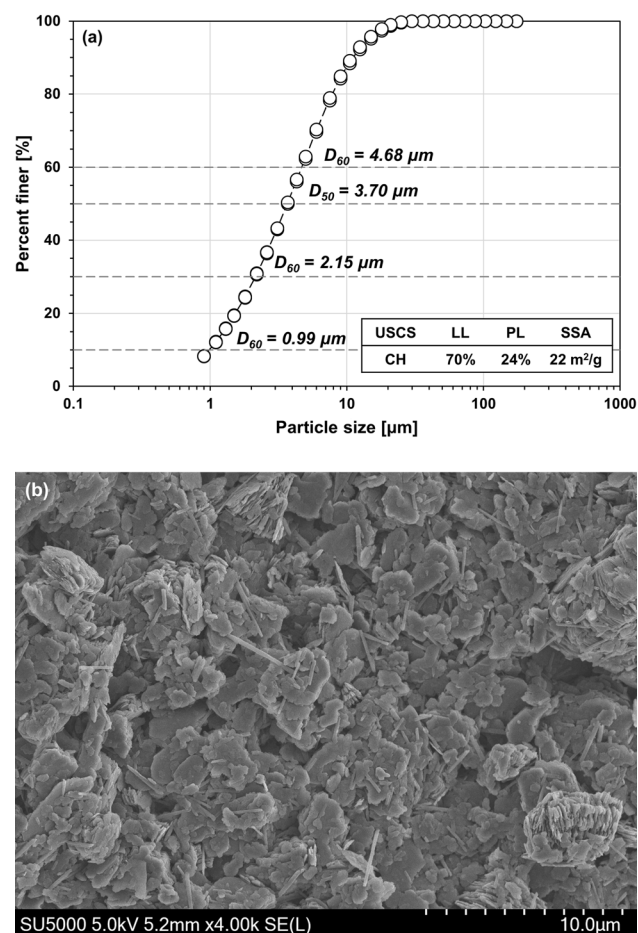

Fig. 1 Basic information of soils used: **a** the particle size distribution curve and **b** the morphology (SEM image) of kaolinite used in this study

kaolinite was dried in an oven at 105 ± 5 °C for at least 24 h to evaporate the pore water [4].

2.1.2 Xanthan gum biopolymer

Among various biopolymers, XG, a high molecular weight polysaccharide secreted by the bacterium *Xanthomonas campestris*, is known to have a minimal impact on the environment and human health [114]. XG is an anionic biopolymer with a linear backbone of 1,4-linked β-D-glucose linked to anionic trisaccharide side chains [20]. Thus, XG can absorb water at approximately 25 times its mass [38] and form electrostatic interactions with soil particles [28]. Moreover, XG possesses pseudoplastic characteristics, wherein its viscosity decreases with increasing shear rates [20]. Thus, XG is commonly used in drug delivery systems [95], food thickening agents [60], and nanoparticle stabilization [89]. In addition, it has been reported that applying XG results in an increase in the soil strength [26, 81] and consistency [28] and causes a decrease in the soil permeability [18]. Other studies have demonstrated the impact of XG on the cyclic performance by offering a longer fatigue life under cyclic loading [82] and a higher damping ratio [51]. For all experimental programs, this study used research-grade XG (CAS No. 11138–66-2; Merck, USA).

2.2 Swelling tests

The swelling pressure of clays was determined using an automatic computerized consolidation test apparatus (Wykeham Farrance; 26-WF3120) with an oedometric cell of 63.5 mm in diameter and 74 mm in height (Wykeham Farrance; 26-WF0321). The porous plate and filter papers (Whatman; Grade 42 filter paper) were placed at the bottom of a specimen ring made of stainless steel with an internal diameter of 63.5 mm and a height of 20 mm. Clay specimens were prepared by mixing dry kaolinite and dry XG (i.e., XG-to-kaolinite mass ratio: m_b/m_s = 0%, 0.5%, 1.0%, and 2.0%). Swelling experiments were conducted under dry conditions to maximize the variation of swelling quantity with XG content. Then, the mixed biopolymer-kaolinite powder was poured into the ring and compacted by tamping in 3 layers to ensure that the mixture can be placed in an oedometric ring. The initial void ratio (e_i = 2.0–2.2) was calculated as $e_i = (G_S \bullet A \bullet h_i - m_s)/G_S$ using the weight of the soil (m_s), the specific gravity of kaolinite (G_S = 2.65), the initial height measured with Vernier calipers (h_i), and the area of the specimen ring (A = 31.67 cm^2). Another porous plate and filter paper were placed above the specimen, allowing deionized water (DI) to flow into the soil from the top and bottom.

Before wetting, specimens were subjected to 5 kPa of vertical loading. Once the sample height was stabilized, DI was poured into the container to initiate specimen wetting. The volumetric expansion due to wetting under consistent confinement (5 kPa) was measured using a top-mounted linear variable displacement transducer (LVDT). Subsequent consolidation tests were conducted at loading increments of 12 kPa, 25 kPa, 50 kPa, 100 kPa, and 200 kPa, and each loading lasted for 24 h. The swelling pressure of the specimen was calculated as the pressure required to restore the initial sample height [9] based on the swelling and consolidation results. The experimental procedures are described in detail in Thakur and Singh [106].

2.3 Consolidation tests

1-D consolidation tests on XG-treated kaolinites (initial water content of 80%) were performed using BS 1377-5 [15] and ASTM D2435 [5]. The porous plates and Whatman Grade 42 filter papers were placed above and below the specimen to allow proper upward and downward drainage during consolidation. The P-wave (PZT plate) and S-wave (bender element) sensors were embedded on the bottom and top plates to simultaneously measure the elastic wave velocities and the specimen height during consolidation. The experimental setup is summarized in Fig. 2.

The experimental specimens were prepared by thoroughly mixing kaolinite, XG, and DI according to the desired kaolinite/XG/water ratios. The consolidation behavior of kaolinites with high water content (80%) was observed to be comparable to that of real-field clays with high water content [116]. Dry XG powder (m_b = 0, 1, and 2 g) was dispersed into the target weight of DI (m_w = 160 g), and uniform XG solutions (XG-to-DI ratio by mass = 0%, 0.625%, and 1.25%) were prepared by mixing

with a magnetic stirrer (DH.WMH03503; Daihan Scientific, Korea). Then, the XG solutions were hand-mixed with kaolinite (m_s = 200 g) to form uniform kaolinite–XG–DI mixture (XG-to-kaolinite ratio by mass = 0%, 0.5%, and 1.0%).

The kaolinite–XG–DI mixture was then placed in an acrylic oedometer cell of diameter 74 mm, after which it was compacted to form an initial height of 45 mm to attain the desired void ratio (i.e., 2.0–2.2, in the same range as that of the swelling experiments). This technique of preparing molded specimens was adopted to avoid specimen disturbance due to cutting and fitting during trimming. Then, the cell was capped with an acrylic top cap, and the oedometer cell with the XG-treated kaolinite specimen was placed on a conventional oedometer testing device.

Vertical loading was applied to the mixture through seven incremental steps (i.e., 12.5, 25, 50, 100, 200, and 400 kPa), whereas untreated kaolinite was loaded up to 200 kPa (i.e., 12.5, 25, 50, 100, and 200 kPa). Then, the vertical stress was reduced by 200 kPa, 100 kPa, and 25 kPa. All vertical loading and unloading steps were maintained until the specimen height varied by less than 0.01 mm for 24 h. Consolidation data were analyzed based on the square-root-of-time (Taylor) method [105]; the void ratio at the end of primary consolidation (e_p) was determined based on the log-of-time (Casagrande) method [19]. The coefficient of consolidation c_v, hydraulic conductivity k, and coefficient of secondary consolidation $c_{\alpha e}$ at each loading step were calculated based on the time–void ratio correlation. The compressibility C_c and swelling index C_S were derived based on the effective stress–void ratios. For the reliability of the experiments, at least two consolidation processes were performed simultaneously for each kaolinite specimen. During the consolidation experiments,
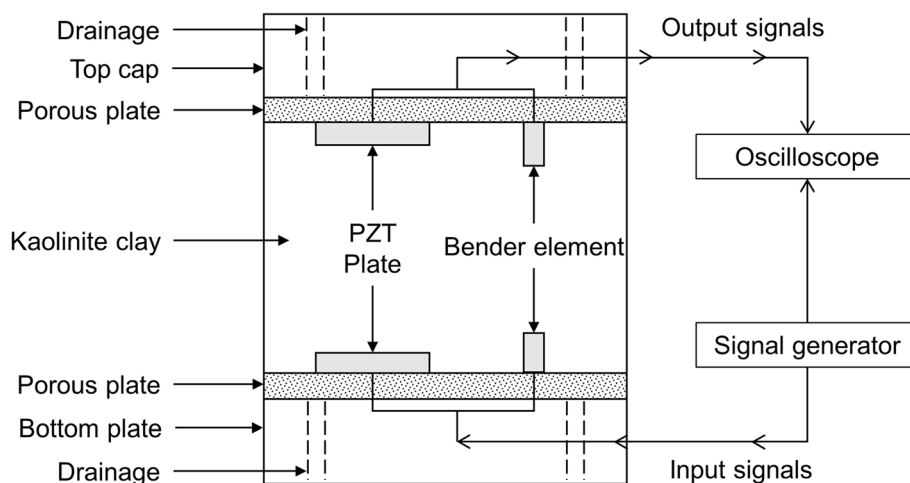

Fig. 2 1D consolidation experimental design with elastic wave measurements

the displacements were measured using a dial gauge with a measurable variation of 0.01 mm.

2.4 Elastic wave measurements

The wave velocities were measured during the consolidation experiments using an oscilloscope (DSOX2014A, Keysight Technologies, USA) and a function generator (33210A, Keysight Technologies, USA). In addition, two different PZT types were embedded at the top and bottom plates of the oedometer cell: plate-type sensors for P-wave measurement and bender-element-type sensors for S-wave measurement. Detailed procedures for sensor production and oedometer cell installation can be found in Chang and Cho [23].

Figure 3 presents an example of the elastic wave signals of the 0.5% XG-treated kaolinite. Single-step signals were generated at the bottom of the PZT sensors (Fig. 3a). The input frequency and amplitude were set to 50 Hz and 10 V for the P-wave and 8 kHz and 10 V for the S-wave. After the first bump, the zero points were handpicked (Fig. 3b) as
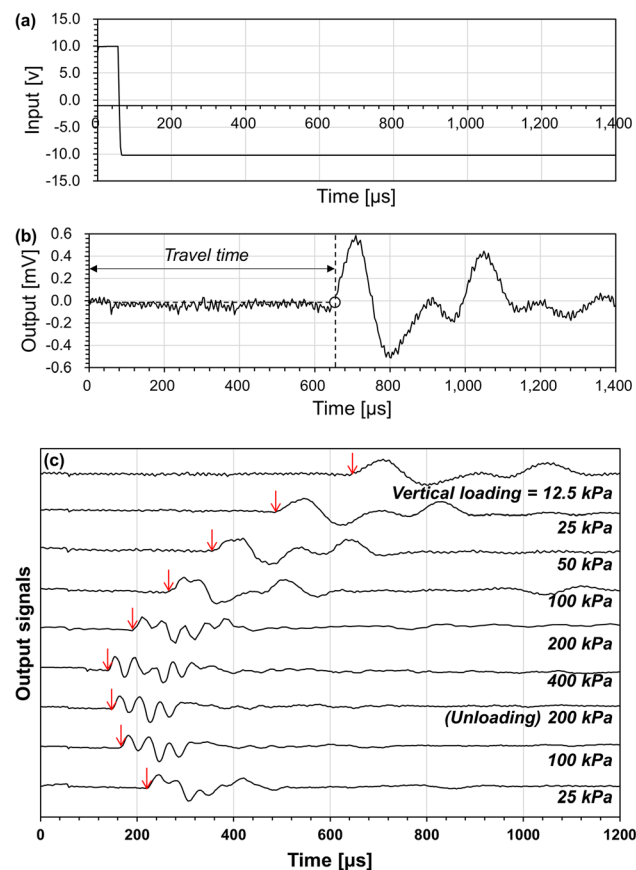

Fig. 3 The S-wave velocity measurements of 0.5% xanthan gum-treated kaolinite; **a** input signal, **b** received signal measured at the end of 12.5 kPa loading, and **c** received signals at the end of each loading step

the arrival time of the S-wave to disregard near-field effects based on Lee and Santamarina [73]. The arrival time decreased with an increase in vertical loading, increased again upon unloading, and was faster than that at the same loading of virgin compression (Fig. 3c). The received raw signals showed a trend similar to a general consolidation curve. Thus, elastic wave measurements can be used to infer the consolidation process of soil.

2.5 Environmental scanning electron microscopy (ESEM)

Environmental SEM is a type of SEM during which the operator can control the water vapor pressure (10–4000 Pa) and the relative humidity in the specimen chamber. Consequently, ESEM allows observation of wet kaolinite by overcoming the shortcomings of traditional SEM, which can only be operated in a vacuum without water. This study utilized ESEM (Quattro S, FEI) to observe the effects of varying humidity on the microstructure of dry XG powder and XG-treated kaolinite. Untreated and 1% XG-treated kaolinites (with the same water content as the consolidation specimen) were sampled and air-dried at room temperature. The specimens were mounted on an ESEM mount. The surface of the specimen was then subjected to electron beams. The relative humidity in the chamber varied from 0 to 100% during observation.

2.6 Unconsolidated and undrained (UU) triaxial tests

UU triaxial compression tests were conducted on XG-treated kaolinites to analyze the effects of XG on the undrained shear strength of kaolinite clays during the consolidation at 50 kPa of vertical loading (i.e., 3.2 m depth) based on the ASTM D2850 standard [7]. The kaolinite powder (m_s = 200 g) was uniformly mixed with 120 g of XG solutions containing different m_b/m_s (i.e., 0.0%, 0.5%, 1.0%, and 2.0%). A membrane suction stretcher wrapped the latex membrane around the soil sample using 10 kPa of suction pressure. The soil specimen was encased in a latex membrane to form a cylinder of height 100 mm and diameter 50 mm. The XG-treated kaolinite was compacted in a latex membrane to obtain the observed void ratio (1.65–1.80) during consolidation at 50 kPa vertical loading. The O-rings on the membrane's top and bottom caps sealed the samples within. The sample volume was then measured after the application of 10 kPa of vacuum pressure to the specimen. The triaxial apparatus was then positioned around the sample, and its cell was filled with de-aired water. The vacuum was slowly released from the kaolinite, while a cell pressure of 10 kPa was applied to maintain the specimen during saturation. The

samples were then saturated with 5 kPa of back pressure until a sample volume (approximately 200 mL) of de-aired water flowed through the system. Lastly, Skempton's B-value was determined by measuring the pore pressure increment induced by increasing the cell pressure, and UU tests were performed on a specimen with a Skempton's B-value greater than 0.9.

Confining pressure (i.e., 50 kPa) was applied after cell assembly without water and air drainage. The specimen was then allowed to rest until a constant pore pressure was established. A motor-driven load frame (HM-5020.3F; Humboldt) sheared the specimens at 1 mm/min (i.e., 1%/min strain) displacement rates. A linearly variable deformation transformer (LVDT) and a load cell mounted on the crosshead of the load frame monitored the axial displacement (in mm) and axial load (in N). Experiments were performed in triplicate for a given confining stress and XG content. The deviator stress at failure was defined using the maximum deviator stress from the stress–strain curve (when a peak value was found) or the deviator stress at an axial strain of 15% (when no peak value was found) while analyzing the stress–strain curves [7].

3 Results and analyses

3.1 Swelling behavior of XG-treated kaolinite

Figure 4a depicts the results of the swelling experiments conducted with a vertical loading of 5 kPa. After water intrusion, untreated kaolinite shows compaction even at 5 kPa because a 1:1 layered clay mineral has a slight swelling potential [31]. Given that the initial water content (i.e., 0%) was lower than optimum water content, the addition of DI results in a change in the clay fabrics to smaller pores [80]. Thus, compaction dominates the swelling of kaolinite following the introduction of water. The compaction behavior also occurred in 0.5% XG and was converted to the swelling phase after approximately 10 min of water flow. In contrast, kaolinite with XG > 1.0% exhibited more significant swelling behavior. The swelling ratio of XG-treated kaolinite increased from 5% (at 0.5% XG) to 20% (at 2.0% XG) because of the fact that hydrophilic XG hydrogels swell by absorbing pore fluids penetrating kaolinite media [16, 103].

When the vertical loading increased, the specimen consolidated, and the volumetric strain decreased, as shown in Fig. 4b. The swelling pressures were determined as effective stress corresponding to zero volumetric strain. Given that vertical compression of 5 kPa dominates the swelling potential of pure kaolinite, XG 0.0% kaolinite exhibited a negative volumetric strain (i.e., compaction) at 5 kPa. XG treatment increased the swelling pressure
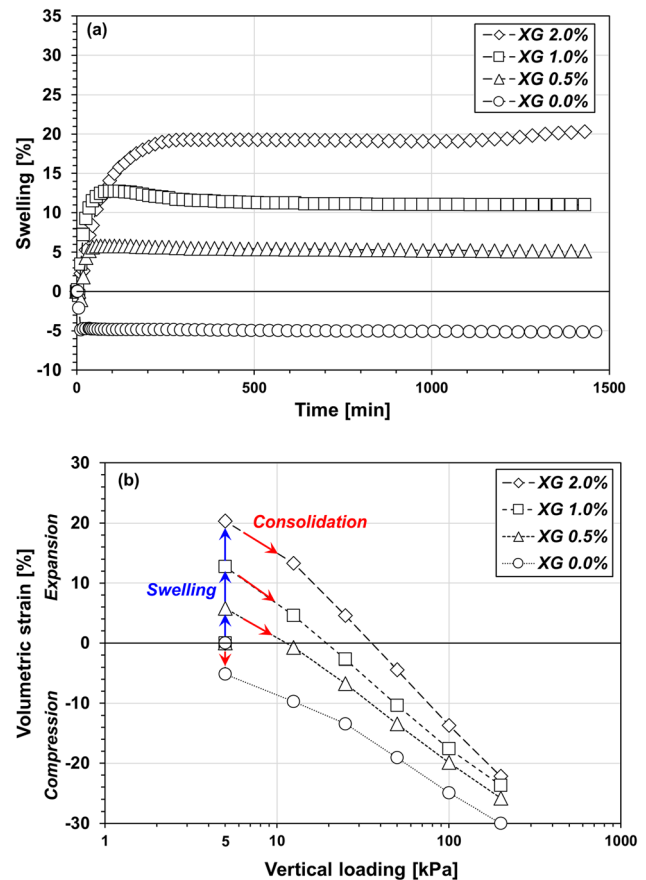

Fig. 4 Swelling and compression characteristics of XG-treated kaolinites; **a** swelling response at 5 kPa, **b** compression characteristics

from < 5 kPa (untreated) to 11.65 kPa (0.5% of XG), 20.35 kPa (1.0% of XG), and 37.70 kPa (2.0% of XG). The final specimen height at each vertical loading was greater than that of the untreated kaolinite, and the slope of the compression curve slightly increased with an increase in XG (Fig. 4b). Typically, clays with high swelling pressure cause instability in civil infrastructure [74]. However, the swelling potentials of XG-treated kaolinite can be applied to improve barrier properties and biodegradability, remediate contaminated soils, provide a buffer for nuclear waste, and maintain borehole stability [2, 65], because of their ability to resist earth pressure loads [101, 102].

3.2 Consolidation behavior of XG-treated kaolinite

Figure 5 shows a semilogarithmic plot of compression curves of the XG-treated kaolinite specimen in terms of e_p versus the effective vertical stress changes. The 0.5% XG-treated kaolinite exhibited the highest e_p among the observed samples, whereas 1.0% XG showed the densest final void ratio. Since kaolinite has negatively charged
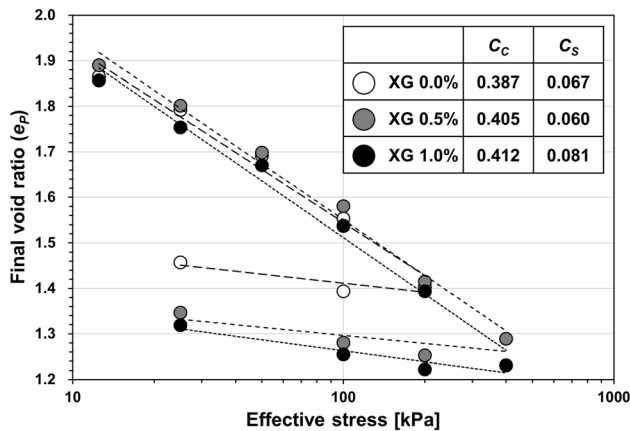
Fig. 5 Compression curves of kaolinite at different XG contents

faces and positively charged edge surfaces [109], XG with anionic charges and kaolinite either repel or attract one another. Electrostatic repulsion between the face surface of kaolinite and anionic XG prevailed at 0.5% XG [56] because of the high face portion of kaolinite [47] and insufficient XG content to form XG-bridges between particles [70], resulting in a greater particle distance. Therefore, 0.5% XG-treated kaolinite showed a larger void ratio than the untreated kaolinite. Chang et al. [28] also noted that 0.5% XG-treated kaolinite showed a local peak liquid limit because XG increased the specific surface area of kaolinite rather than forming bridges between clay particles.

In contrast, because of the bonding between kaolinite and XG, 1.0% XG-treated kaolinite showed a denser ep, even at low vertical stress. XG forms interparticle bonds directly with positively charged edge surfaces and indirectly with face surfaces via hydrogen bonds [104, 117]. XG-induced particle bonding aggregates kaolinite particles, resulting in a decrease in e_p. In addition, XG-adsorbed water was expelled by increased vertical loading, reducing e_p with increasing XG content.

Both C_C and C_S increased with increasing XG content, as shown in the legend in Fig. 5. This is because the repulsion force between XG and the surface of kaolinite was overcome by the increase in vertical loading, which further resulted in a marginal increase in the rate of change of e_p for XG-treated kaolinite as compression stress increased. Moreover, XG is more sensitive to volume change due to vertical load variation because it contains a large amount of water [38].

$C_{\alpha e}$ is the void ratio variation over the log of time starting after the primary consolidation [80]. Secondary compression occurs by water discharge from the micropores in an adsorbed state, and the continuous skeletal deformation of soils occurs during primary consolidation [113], which is dependent on complex factors such as

particle rearrangement, pre-consolidation pressure, and stress history [45]. For instance, in XG-treated kaolinite (Fig. 6), water strongly adsorbed by XG was slowly discharged during the secondary consolidation process, resulting in fabric rearrangement and a proportionally higher $C_{\alpha e}$ to the XG content. Here, $C_{\alpha e}$ increased with the effective stress for both untreated and 0.5% XG-treated kaolinite because a greater vertical loading accelerated the discharge of adsorbed water. In contrast, $C_{\alpha e}$ of 1.0% XG-treated kaolinite gradually decreased as the effective stress increased because XG-induced bridges became compact as the vertical pressure increased [34].

3.3 Permeability of XG-treated kaolinite

The c_v is related to the rate of 1D consolidation when saturated kaolinite is exposed to increased vertical pressure. Overall, c_v increased as e_p declined (Fig. 7a). For the same soil specimen, e_p is inversely proportional to effective stress, and c_v is expected to increase with effective stress [115]. Furthermore, c_v decreases with an increase in the coefficient of volume change, whose value increases with e_p [39]. The c_v value for untreated kaolinite falls within the range of $8–30 \times 10^{-4}$ cm/s, which is consistent with the previously reported c_v value for kaolinite [59, 91]. XG treatment reduced the c_v of kaolinite soils by 52.60% (0.5% XG at 100 kPa) to 98.87% (1.0% XG at 12.5 kPa) compared to that of untreated kaolinite at the same vertical effective stress.

The permeability (k) of kaolinite at e_p was computed using the relationship between c_v and k (i.e., $k = c_v m_v \gamma_w$). The log k increases linearly with an increase in e_p owing to the larger drainage paths. The k of the XG-treated kaolinite decreased exponentially during the consolidation stages, from untreated kaolinite ($1.5–11.8 \times 10^{-7}$ cm/s) to 0.5% XG-treated kaolinite ($0.07–3.8 \times 10^{-7}$ cm/s) and 1% XG-
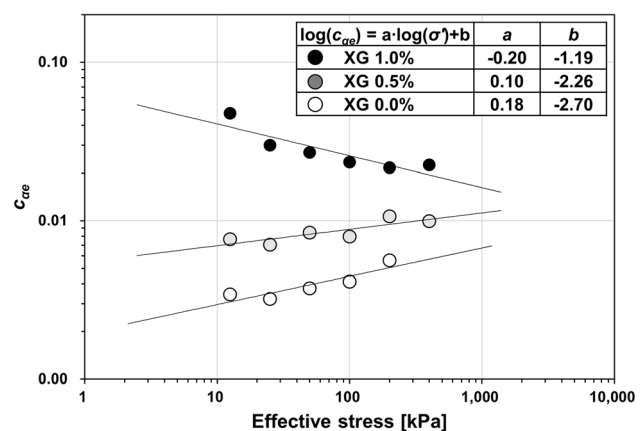

Fig. 6 Xanthan gum effect on the coefficient of secondary compression with various effective stresses
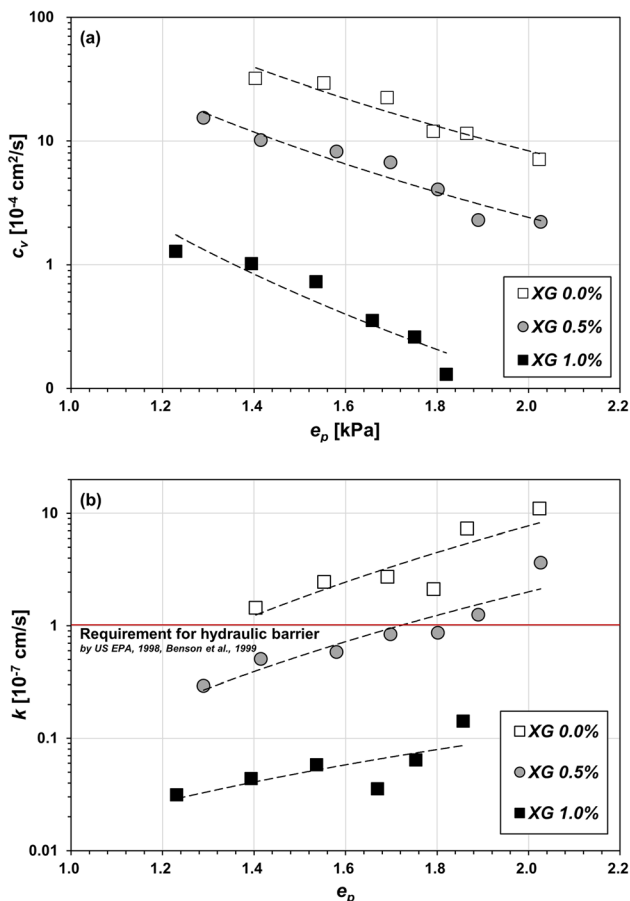
Fig. 7 Variation in **a** the coefficient of consolidation and **b** the hydraulic conductivity with a variation in the void ratio at the end of primary consolidation

Fig. 8 The variation in **a** P-wave and **b** S-wave velocity with void ratio

treated kaolinite (0.04–0.15×10^{-7} cm/s) as shown in Fig. 7b. The decrease in k was caused by the clogging of pore space by viscous XG hydrogels.

3.4 Wave velocity variation during consolidation

Figure 8 summarizes the results of the elastic wave velocity measured during the consolidation procedures at vertical effective stresses ranging from 12.5 kPa to 200 kPa. The P-wave velocity (V_P) is typically higher than the S-wave velocity (V_S) under identical conditions (e.g., void ratio and effective stress). Both V_P and V_S decreased with an increase in the void ratio because kaolinite particles were initially loosely packed with a higher void ratio. Figure 8a shows no significant relationship between the V_P and XG content. However, V_S (Fig. 8b) decreases with increasing XG content. The V_S difference with XG addition is more significant at a higher void ratio than with a lower void ratio.

The parameters a and b obtained from the wave velocity and void ratio relationships are also depicted in Fig. 8,
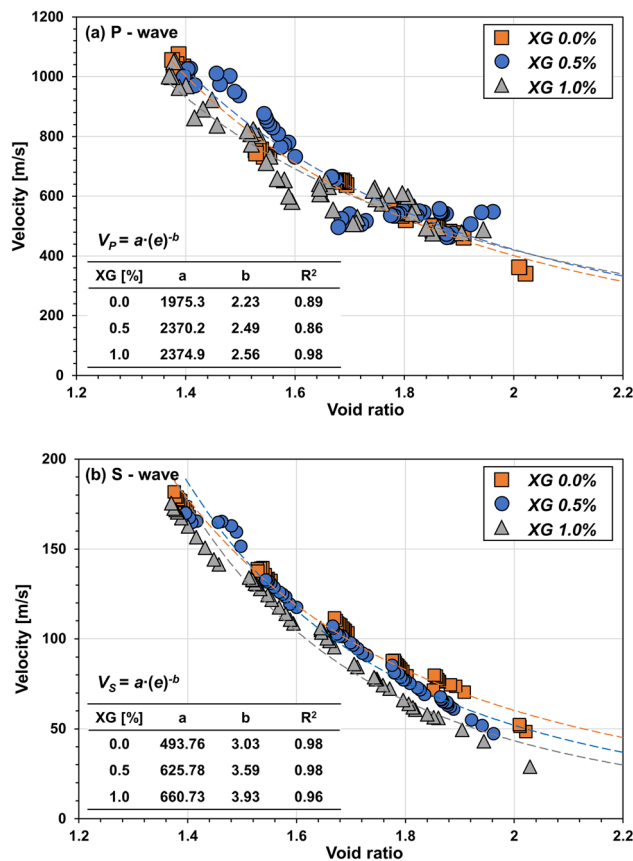
where parameter a indicates the wave velocity at a void ratio of 1 and b represents the sensitivity of wave velocity to the variation in void ratio. Both a and b tended to increase with XG treatment, whereas the S-wave velocity showed a more significant variation. The results indicate that XG has a more prominent effect on the shear stiffness than on the bulk stiffness of the kaolinites.

If the distance between kaolinite particles is insufficient for an XG-bridge (i.e., high void ratio), the repulsive forces between the negatively charged XG and kaolinite prevail [117], resulting in a decrease in effective stress and the V_S [55]. As the void ratio decreases, XG and kaolinite form face-to-face-like fabrics through direct electrostatic bonding with the positive edge surface and hydrogen bonding with the face surface [108]. Thus, the V_S of XG-treated kaolinite would be comparable to that of untreated kaolinite. However, even in such instances, kaolinite–XG–kaolinite contact resulted in a slightly lower V_S for XG-treated kaolinite.

Figure 9 illustrates the variation in V_P and V_S of XG-treated kaolinite subjected to a vertical loading of 200 kPa, in terms of the velocity ratio (i.e., the wave velocity ratio to that at 0 s). The elastic wave velocity increased
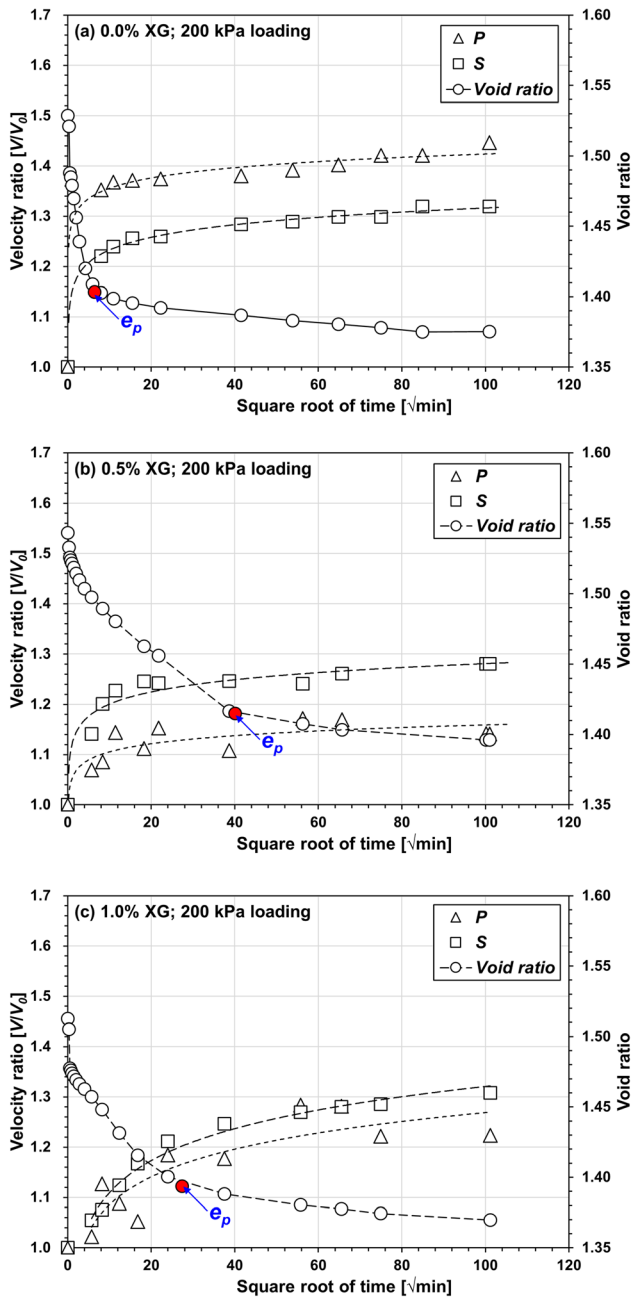
Fig. 9 Variation in the wave velocity and void ratio during a 200 kPa loading for **a** untreated, **b** 0.5% XG-treated, and **c** 1.0% XG-treated kaolinites

logarithmically with the square root of time. Although V_P and V_S increased slightly during the secondary consolidation, most of the V_P and V_S increases were completed during the primary consolidation, indicating that pore fluid dissipation during the primary consolidation causes an increase in effective stress. In contrast, the increase in effective stress during secondary consolidation is relatively modest, but it must be considered, especially for XG-treated kaolinites. The initial V_P and V_S increased slowly

with XG treatment because XG delayed primary consolidation. Notably, XG treatment increased V_P and V_S more steeply during the secondary consolidation process.

Figure 10 depicts the variation in V_P and V_S measured at the end of primary consolidation. The analysis differentiates between the loading and unloading stages because of the different stress paths and fabrics. During the loading stages, the V_P was marginally affected by the XG content, whereas the V_S at the same effective stress decreased gradually with XG. The V_P and V_S dropped during unloading but were still higher than those at the same vertical effective stress of virgin compression. Compared to untreated kaolinite, the XG treatment resulted in a minor variation in V_P and V_S during the unloading process.

The correlation between wave velocities and the void ratio based on Eq. 1 [21] is summarized in Table 1.

$$v = \alpha\left(\sigma_v'\right)^{\beta} \tag{1}$$

where σ_v' represents the vertical effective stress, and α and β are experimentally determined parameters. Parameter α indicates the wave velocity at the vertical effective stress of 1 kPa, and β captures the sensitivity of the kaolinite stiffness to the applied stress. Parameter α of the P-wave
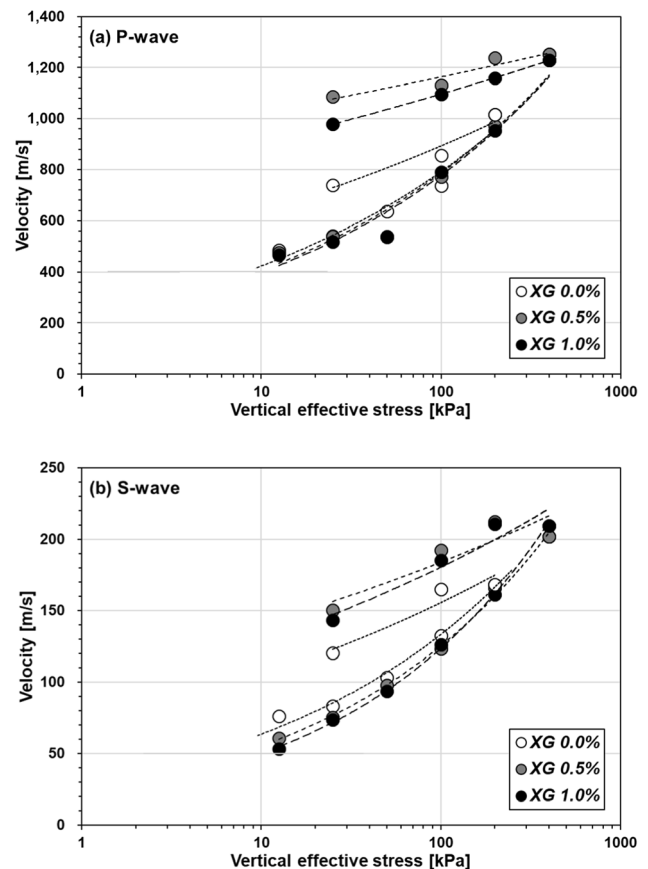

Fig. 10 Wave velocity of XG-treated kaolinites at the end of primary consolidation; **a** P-wave velocity and **b** S-wave velocity

Table 1 Parameters obtained from the correlation between the vertical effective stress and wave velocity

Wave type	XG	Loading			Unloading		
		α	β	R^2	α	β	R^2
P-wave	0.0	226.35	0.27	0.98	455.67	0.15	0.94
	0.5	210.06	0.29	0.94	875.57	0.06	0.92
	1.0	203.50	0.29	0.95	752.84	0.08	1.00
S-wave	0.0	30.51	0.32	0.98	63.50	0.20	0.99
	0.5	24.59	0.35	1.00	93.38	0.15	0.99
	1.0	20.43	0.39	1.00	83.55	0.17	0.99

slightly decreased (up to 10%) with XG treatment during loading, whereas β slightly increased. However, α of the S-wave demonstrated a greater decrease (up to 30%), and β increased with XG from 0.32 to 0.39. The wave velocity and α decreased because the repulsive force between XG and kaolinite inhibited the contact between kaolinite particles [57]. In addition, the bond between XG and kaolinite produces FF-like kaolinite fabrics, resulting in wave propagation through the connection between kaolinite and XG. Previous studies by Faris et al. [42] also stated that V_S traveling through hydrogel media was less than 1 m/s. A rise in β with XG indicates that XG contributes to a more significant increase in stiffness as vertical loading increases. The difference in the XG effect on P- and S-waves seems to be due to the contribution of XG to the elastic modulus (shear modulus and bulk modulus) of kaolinites [83]. The shear modulus of kaolinite (i.e., 2–37 MPa, calculated from V_S in this study) is comparably lower than that of the bulk modulus of kaolinite (i.e., 180–1913 MPa, calculated from V_P in this study) and water (i.e., approximately 2200 MPa [79]). Thus, the XG contribution was more pronounced for S-wave propagation. Previous studies also pointed out that the biopolymer treatment significantly affected the V_S and slightly affected the V_P [22, 83]. During the unloading stages, the parameter α increased with the XG content because of its higher pre-consolidation stress, whereas β decreased to 60% of the untreated kaolinite. The smaller β of XG at the unloading stage suggests that XG treatment may contribute to maintaining stiffness when the upper load is removed during excavation, erosion, or other soil loss.

3.5 Amplitude analysis

Figure 11 depicts a remarkable reduction in the P-wave and a slight reduction in the S-wave amplitude as a result of XG treatment. Peak-to-peak amplitude values were calculated across the widowed waveforms for the first cycle. The
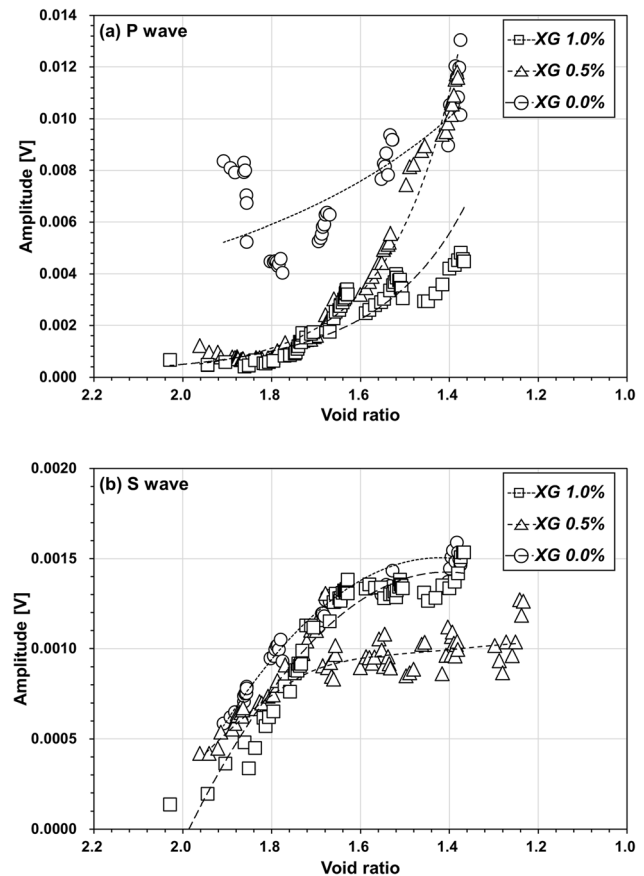
Fig. 11 Amplitude changes of **a** P-wave and **b** S-wave obtained from the consolidation experiments with XG treatment

amplitude increased as the void ratio decreased because the travel path of the waves shortened during the consolidation process. The received P-wave signals have higher amplitudes than the S-wave signals because of their lower frequencies. Signals with higher frequencies typically oscillate during wave propagation, which results in considerable energy loss [83].

The average P-wave amplitude decreased from 7.63 mV (untreated) to 4.07 mV (0.5% XG) and 2.46 mV (1.0% XG), whereas the average S-wave amplitude was 1.18 mV (untreated) to 0.87 mV (0.5% XG). The phase differences between rigid kaolinite particles and ductile XG gels result in energy dissipation at the XG–kaolinite interfaces and XG hydrogels [51]. In addition, structural disturbance (i.e., particle dispersion via repulsive forces between the kaolinite face and XG, FF-like particle bonding via attractive force between kaolinite edge and XG) occurred through XG–kaolinite interaction, resulting in higher energy dissipation during the wave propagations.

4 Discussion

4.1 Behavior of XG-treated kaolinites during consolidation process based on microscopic observations

The ESEM observation of the XG molecule revealed a swelling characteristic of XG as relative humidity increased from 7.1% (Fig. 12a) to 100.0% (Fig. 12b). As shown, the volume of XG increased upon the absorption of adjacent water molecules. The ESEM results showed a 1.2-fold increase in length following the water adsorption, which can be approximated to represent a 1.4-fold and 1.7-fold increase in surface area and volume, respectively. In addition, the electrostatic interaction between kaolinite and XG affected the consolidation behavior by re-arranging kaolinite particles. XG encouraged kaolinite into FF-like fabrics via a repulsive force between the face surface and XG and via electrostatic attraction force between the edge surface and XG, as shown in Fig. 12c. With increased relative humidity (Fig. 12d), XG-adsorbed water and formed viscous hydrogels.

The swelling of XG in the void space (Fig. 4a) resisted consolidation pressure. Thus, XG-treated kaolinite showed a higher void ratio in the swelling experiments (Fig. 4b)

than 0.5% XG-treated kaolinite in the consolidation experiment (Fig. 5). Adsorbed water squeezed out at vertical stress higher than the swelling potential of XG. Both factors resulted in a larger C_C (Fig. 5). When the applied load was removed, XG-adsorbed water and swelled again, showing a higher C_S than the untreated kaolinite (Fig. 5). The volume-expanded XG clogged void spaces and inhibited water drainage, drastically lowering k and c_v with XG treatment (Fig. 7). With increased relative humidity, XG surrounding the kaolinite surface formed a viscous hydrogel by absorbing pore fluids and swelling, which reduced direct kaolinite-to-kaolinite contact. Thus, V_S decreased with XG content (Fig. 8b), whereas V_P changed slightly with XG content (Fig. 8a). Wave propagation through the ductile XG hydrogel resulted in more significant energy dissipation (Fig. 11).

4.2 Possible applications of XG in terms of consolidation

Figure 13a depicts the stress–strain curves from the unconfined undrained triaxial tests of kaolinite under different XG conditions, where the initial void ratio for each example was in the range of 1.72 ± 0.005. Although the deviator stress of untreated kaolinite became constant at
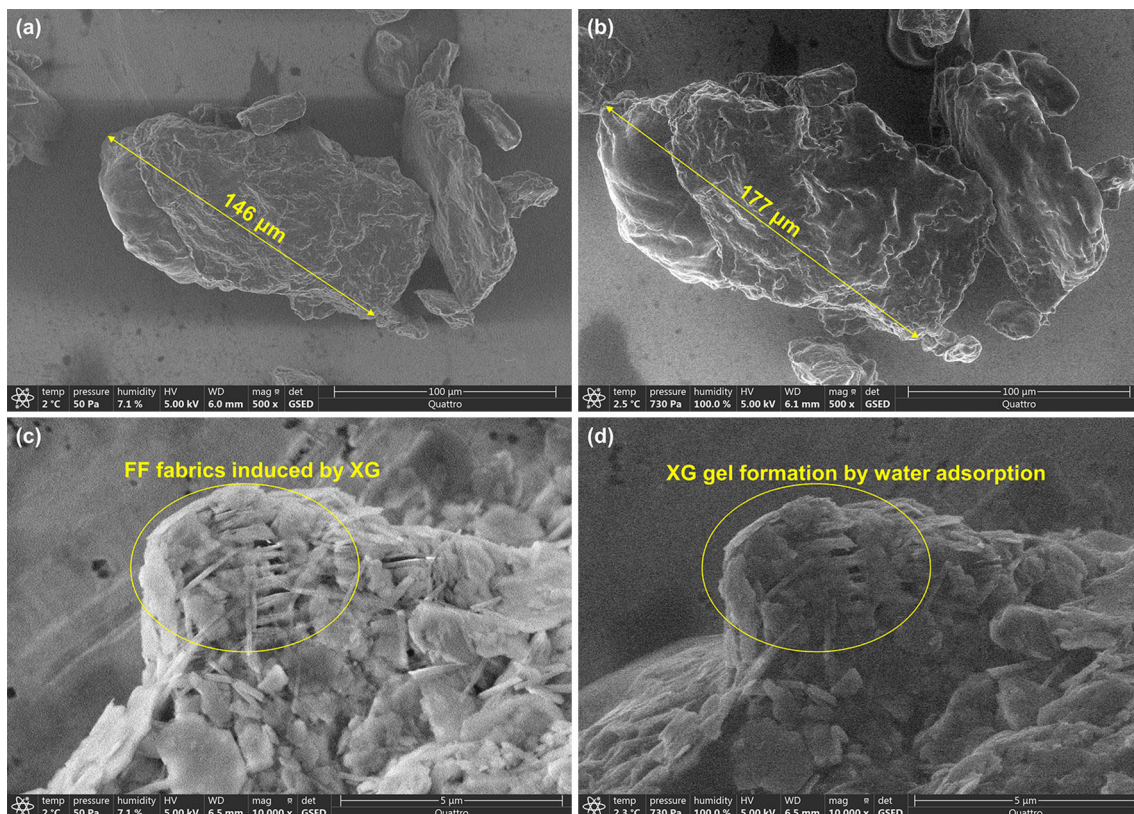

Fig. 12 ESEM images of xanthan gum (**a, b**) and XG-treated kaolinite (**c, d**) with a variation of relative humidity from 7.1% (**a, c**) to 100% (**b, d**)
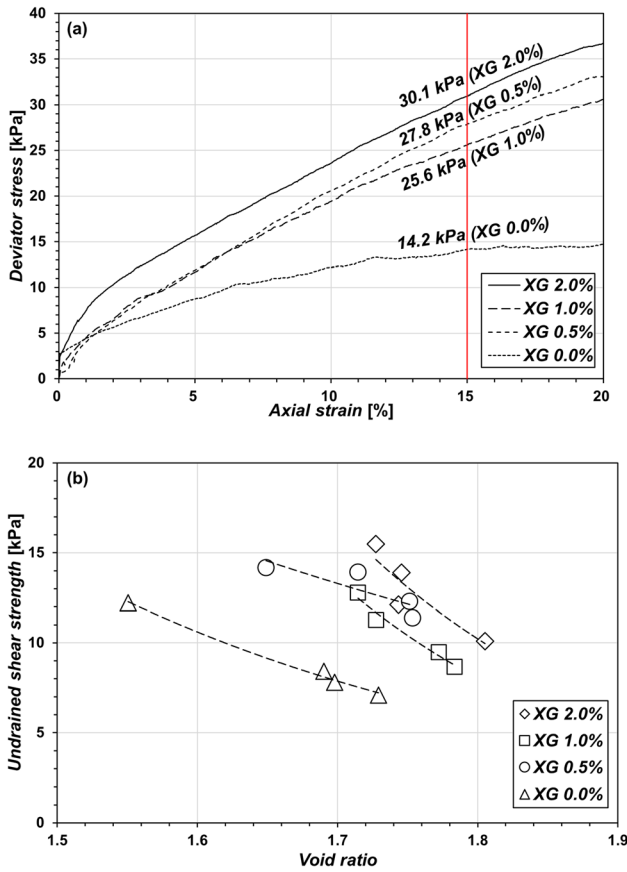
Fig. 13 UU triaxial results of XG-treated kaolinites: **a** stress–strain relation at void ratio of 1.72 ± 0.005 and **b** undrained shear strength at different void ratios

approximately 15% axial strain, the axial strain of the XG-treated specimen reached 15% without exhibiting a peak value. According to the ASTM D2850 standard [7], the deviator stress at failure was determined as the deviator stress at an axial strain of 15% for all specimens. The XG treatment caused the deviator stress at failure to increase from 14.2 kPa (untreated) to 30.1 kPa (XG 2.0%). The improvement in stress–strain behavior was comparable between 0.5% (27.8 kPa) and 1.0% (25.6 kPa) of XG, and further enhancement was observed at 2.0% of XG. Several hypotheses could account for the increase in shear resistance caused by applying XG. First, the bonding between XG and kaolinite particles improves particle contact and shear strength [36]. Moreover, the XG-induced FF particle alignment is stronger than the EF particle contact [92]. Lastly, an increase in the pore fluid viscosity due to XG enhances the resistance of soil to shear force [86]. Figure 13b depicts the improvement in s_u, which is defined as half of the deviator stress at failure, as a function of the void ratio. By altering the log–log relationship between s_u and the void ratio [27, 66], the interactions between XG, kaolinite, and pore fluids led to a more than twofold rise in

s_u (from 7.43 kPa (untreated) to 15.20 kPa (2% XG) at $e = 1.72$), whereas s_u at $e = 1.72$ was calculated to be 12.81 kPa for 0.5% XG and 12.13 kPa for 1.0% XG.

Figure 14 compares the estimated s_u derived from the log–log relationship between s_u and e in Fig. 13b to the consolidation curves for a vertical loading of 50 kPa (i.e., an estimated depth of 3.2 m). Even with a higher void ratio, XG-treated kaolinite exhibited a higher s_u (from 10 to 16 kPa) than untreated kaolinite (ranging from 6–9 kPa).
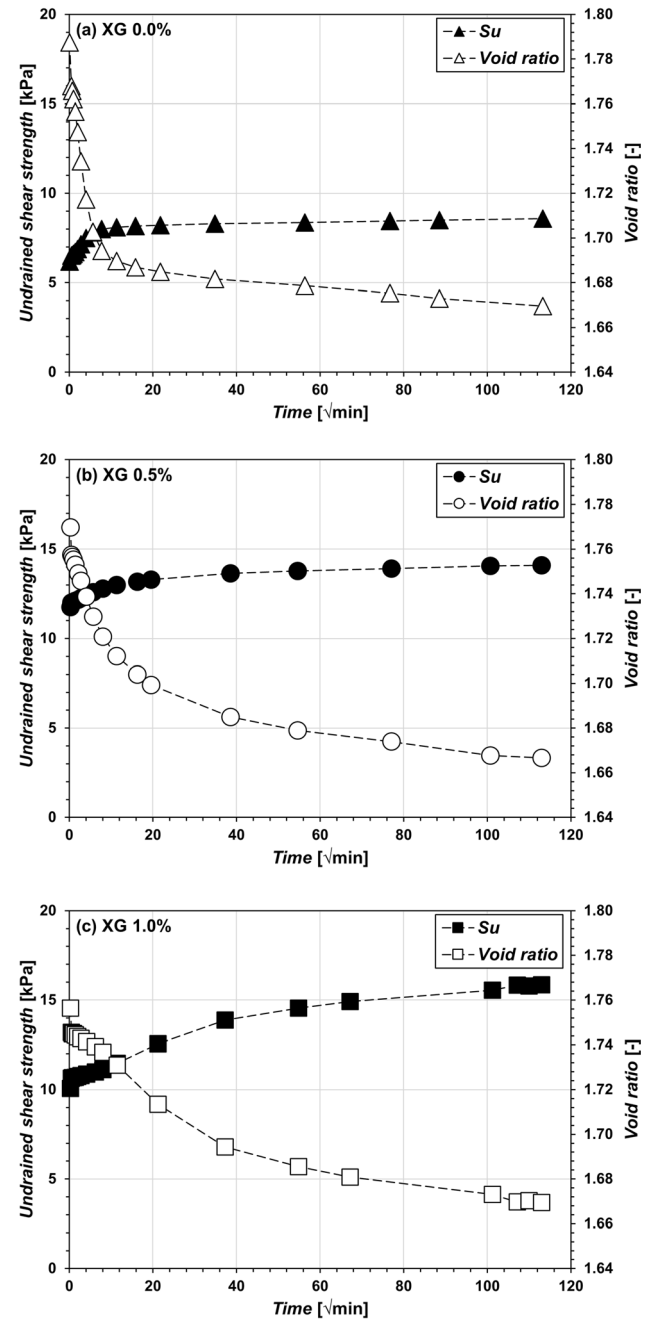

Fig. 14 Estimated undrained shear strength during consolidation at 50 kPa of vertical loading for **a** untreated kaolinite, **b** 0.5% XG-treated kaolinite, and **c** 1.0% XG-treated kaolinite

In other words, the XG treatment for kaolinite reduces the overall consolidation time necessary to achieve a capacity of soft soil to withstand loads applied to the ground above, including the construction equipment for soft soil stabilization (e.g., dozer, crane) [63, 64]. However, the application of XG to kaolinite has both limitations and advantages in terms of the consolidation. The swelling pressure of XG and the interaction force between XG and kaolinite have the potential to resist the vertical consolidation forces. However, a thorough evaluation of XG content is required because a higher XG content resulted in a higher C_C and $C_{\alpha e}$ due to the squeezing out of water adsorbed by XG, and a lower C_V delays the consolidation procedure. Thus, further studies should be conducted to consider additional drainage methods after obtaining a higher s_u by XG treatment. Furthermore, cations in soils should be considered because they can promote XG adsorption on kaolinite and decrease soil compressibility [46].

In addition to consolidation purposes, XG in pore spaces absorbs water, swells, and clogs pore spaces, resulting in a hindered water flow along with the pore spaces. The water-holding and pore-clogging capacity of XG increased as its content rose. Therefore, XG-treated kaolinite has the potential to be used as a hydraulic barrier, as it meets the requisite k value of less than 10^{-7} cm/s [12, 110], allowing the use of kaolinite, which is widely distributed compared to conventional hydraulic barrier materials such as bentonite. Lastly, an increase in P- and S-wave attenuation after XG treatment suggests that XG could be utilized for seismic stabilization of the ground.

5 Conclusions

This study investigated the effect of xanthan gum treatment on the swelling, compressibility, permeability, elastic wave propagation, and undrained shear strength during the consolidation of high-water-content kaolinite clays. XG biopolymer affected the consolidation and swelling behavior of soils as a result of the absorption of pore fluids, the development of XG–kaolinite bonds, and the repulsion of kaolinite particles. The XG-induced water absorption increased the swelling pressure and swelling indices of kaolinite, demonstrating its potential to provide a barrier or buffer, enable the remediation of contaminated soils, and assist in the maintenance of borehole stability. The void ratio at the end of primary consolidation varied slightly depending on the XG content. Given the dominant repulsive force between XG and kaolinite, 0.5% of XG exhibited a higher void ratio. Further, 1.0% of XG exhibited a lower void ratio because of the formation of XG-bridges

between kaolinites. The compressibility and swelling index marginally increased after applying the XG treatment.

The XG-treated kaolinite, by contrast, exhibited significant energy dissipation during the propagation of an elastic wave, demonstrating the potential of XG for seismic stabilization. In addition, the XG hydrogel clogged the pore spaces and drastically reduced the hydraulic conductivity, meeting the criteria for use as a hydraulic barrier and landfill lining material. Lastly, the XG treatment increased s_u at the same consolidation period, which can further minimize the consolidation time required for construction equipment to enter the soft ground. These results revealed the potential of XG application for the stabilization of fine-grained soils with high water content for controlling hydraulic conductivity, seismic stabilization, and rapid surface stabilization for the trafficability of construction equipment. If additional drainage is not considered, a low XG content should be used in practical applications.

Availability of data and materials All data, models, and code generated or used during the study appear in the published article.

Declarations

Conflict of interest The authors declare that they have no conflicts of interest that could have influenced the work reported in this paper.

References

1. Almajed A, Lemboye K, Arab MG, Alnuaim A (2020) Mitigating wind erosion of sand using biopolymer-assisted EICP technique. Soils Found 60(2):356–371. https://doi.org/10.1016/j.sandf.2020.02.011

2. Anderson RL, Ratcliffe I, Greenwell HC, Williams PA, Cliffe S, Coveney PV (2010) Clay swelling—a challenge in the oilfield. Earth Sci Rev 98(3):201–216. https://doi.org/10.1016/j.earscirev.2009.11.003

3. ASTM (2020) B822-20: standard test method for particle size distribution of metal powders and related compounds by light

scattering. ASTM International, West Conshohocken. https://doi.org/10.1520/B0822-20

4. ASTM (2019) D2216–19: standard test methods for laboratory determination of water (moisture) content of soil and rock by mass. ASTM International, West Conshohocken. https://doi.org/10.1520/D2216-19

5. ASTM (2020) D2435: standard test methods for one-dimensional consolidation properties of soils using incremental loading. ASTM International, West Conshohocken. https://doi.org/10.1520/D2435_D2435M-11R20

6. ASTM (2017) D2487–17: standard practice for classification of soils for engineering purposes (Unified Soil Classification System). ASTM International, West Conshohocken. https://doi.org/10.1520/D2487-17

7. ASTM (2015) D2850: standard test method for unconsolidated-undrained triaxial compression test on cohesive soils. ASTM International, West Conshohocken. https://doi.org/10.1520/D2850-15

8. ASTM (2020) D4464-15: standard test method for particle size distribution of catalytic materials by laser light scattering. ASTM International, West Conshohocken. https://doi.org/10.1520/D4464-15R20

9. ASTM (2021) D4546–21: standard test methods for one-dimensional swell or collapse of soils. ASTM International, West Conshohocken. https://doi.org/10.1520/D4546-21

10. Ayeldeen M, Negm A, El-Sawwaf M, Kitazume M (2017) Enhancing mechanical behaviors of collapsible soil using two biopolymers. J Rock Mech Geotech Eng 9(2):329–339. https://doi.org/10.1016/j.jrmge.2016.11.007

11. Ayeldeen MK, Negm AM, El Sawwaf MA (2016) Evaluating the physical characteristics of biopolymer/soil mixtures. Arab J Geosci 9(5):1–13. https://doi.org/10.1007/s12517-016-2366-1

12. Benson CH, Daniel DE, Boutwell GP (1999) Field performance of compacted clay liners. J Geotech Geoenviron 125(5):390–403. https://doi.org/10.1061/(ASCE)1090-0241(1999)125:5(390)

13. Bouazza A, Gates W, Ranjith P (2009) Hydraulic conductivity of biopolymer-treated silty sand. Géotechnique 59(1):71–72. https://doi.org/10.1680/geot.2007.00137

14. Bozyigit I, Javadi A, Altun S (2021) Strength properties of xanthan gum and guar gum treated kaolin at different water contents. J Rock Mech Geotech Eng 13(5):1160–1172. https://doi.org/10.1016/j.jrmge.2021.06.007

15. British Standard Institute (1990) BS 1377-5: methods of test for soils for civil engineering purposes. Compressibility, permeability and durability tests. British Standard Institute. https://doi.org/10.3403/00211981

16. Bueno VB, Bentini R, Catalani LH, Petri DFS (2013) Synthesis and swelling behavior of xanthan-based hydrogels. Carbohyd Polym 92(2):1091–1099. https://doi.org/10.1016/j.carbpol.2012.10.062

17. Cabalar AF, Awraheem MH, Khalaf MM (2018) Geotechnical properties of a low-plasticity clay with biopolymer. J Mater Civ Eng 30(8):04018170. https://doi.org/10.1061/(ASCE)MT.1943-5533.0002380

18. Cabalar AF, Wiszniewski M, Skutnik Z (2017) Effects of xanthan gum biopolymer on the permeability, odometer, unconfined compressive and triaxial shear behavior of a sand. Soil Mech Found Eng 54(5):356–361. https://doi.org/10.1007/s11204-017-9481-1

19. Casagrande A, Fadum RE (1940) Notes on soil testing for engineering purposes. Harvard University, Cambridge

20. Casas JA, Santos VE, Garcia-Ochoa F (2000) Xanthan gum production under several operational conditions: molecular structure and rheological properties. Enzyme Microb Technol 26(2):282–291. https://doi.org/10.1016/S0141-0229(99)00160-X

21. Cha M, Santamarina JC, Kim H-S, Cho G-C (2014) Small-strain stiffness, shear-wave velocity, and soil compressibility. J Geotech Geoenviron 140(10):06014011. https://doi.org/10.1061/(ASCE)GT.1943-5606.0001157

22. Chang I, Cho G-C (2014) Geotechnical behavior of a beta-1,3/1,6-glucan biopolymer-treated residual soil. Geomech Eng 7(6):633–647. https://doi.org/10.12989/gae.2014.7.6.633

23. Chang I, Cho G-C (2010) A new alternative for estimation of geotechnical engineering parameters in reclaimed clays by using shear wave velocity. Geotech Test J 33(3):171–182. https://doi.org/10.1520/GTJ102360

24. Chang I, Im J, Cho GC (2016) Introduction of microbial biopolymers in soil treatment for future environmentally-friendly and sustainable geotechnical engineering. Sustainability 8(3):251. https://doi.org/10.3390/su8030251

25. Chang I, Im J, Lee S-W, Cho G-C (2017) Strength durability of gellan gum biopolymer-treated Korean sand with cyclic wetting and drying. Constr Build Mater 143:210–221. https://doi.org/10.1016/j.conbuildmat.2017.02.061

26. Chang I, Im J, Prasidhi AK, Cho G-C (2015) Effects of xanthan gum biopolymer on soil strengthening. Constr Build Mater 74:65–72. https://doi.org/10.1016/j.conbuildmat.2014.10.026

27. Chang I, Kwon Y-M, Cho G-C (2021) Effect of pore-fluid chemistry on the undrained shear strength of xanthan gum biopolymer-treated clays. J Geotech Geoenviron 147(11):06021013. https://doi.org/10.1061/(ASCE)GT.1943-5606.0002652

28. Chang I, Kwon Y-M, Im J, Cho G-C (2019) Soil consistency and interparticle characteristics of xanthan gum biopolymer–containing soils with pore-fluid variation. Can Geotech J 56(8):1206–1213. https://doi.org/10.1139/cgj-2018-0254

29. Chang I, Lee M, Tran ATP, Lee S, Kwon Y-M, Im J, Cho G-C (2020) Review on biopolymer-based soil treatment (BPST) technology in geotechnical engineering practices. Transp Geotech 24:100385. https://doi.org/10.1016/j.trgeo.2020.100385

30. Chang I, Prasidhi AK, Im J, Cho G-C (2015) Soil strengthening using thermo-gelation biopolymers. Constr Build Mater 77:430–438. https://doi.org/10.1016/j.conbuildmat.2014.12.116

31. Chavali RVP, Reddy P (2018) Volume change behavior of phosphogypsum treated clayey soils contaminated with inorganic acids—a micro level study. J Environ Eng Landsc 26:8–18. https://doi.org/10.3846/16486897.2017.1331168

32. Chen R, Lee I, Zhang L (2015) Biopolymer stabilization of mine tailings for dust control. J Geotech Geoenviron 141(2):04014100. https://doi.org/10.1061/(ASCE)GT.1943-5606.0001240

33. Chen R, Zhang L, Budhu M (2013) Biopolymer stabilization of mine tailings. J Geotech Geoenviron 139(10):1802–1807. https://doi.org/10.1061/(ASCE)GT.1943-5606.0000902

34. Cheng G, Zhu H-H, Wen Y-N, Shi B, Gao L (2020) Experimental investigation of consolidation properties of nano-bentonite mixed clayey soil. Sustainability 12(2):459. https://doi.org/10.3390/su12020459

35. Choi S-G, Chang I, Lee M, Lee J-H, Han J-T, Kwon T-H (2020) Review on geotechnical engineering properties of sands treated by microbially induced calcium carbonate precipitation (MICP) and biopolymers. Constr Build Mater 246:118415. https://doi.org/10.1016/j.conbuildmat.2020.118415

36. Dehghan H, Tabarsa A, Latifi N, Bagheri Y (2019) Use of xanthan and guar gums in soil strengthening. Clean Technol Environ Policy 21(1):155–165. https://doi.org/10.1007/s10098-018-1625-0

37. DeJong JT, Soga K, Kavazanjian E, Burns S, Paassen LAV, Qabany AA, Aydilek A, Bang SS, Burbank M, Caslake LF,

Chen CY, Cheng X, Chu J, Ciurli S, Esnault-Filet A, Fauriel S, Hamdan N, Hata T, Inagaki Y, Jefferis S, Kuo M, Lalaoui L, Larrahondo J, Manning DAC, Martinez B, Montoya BM, Nelson DC, Palomino A, Renforth P, Santamarina JC, Seagren EA, Tanyu B, Tsesarsky M, Weaver T (2013) Biogeochemical processes and geotechnical applications: progress, opportunities and challenges. Géotechnique 63(4):287–301. https://doi.org/10.1680/geot.SIP13.P.017

38. Dogan M, Toker OS, Goksel M (2011) Rheological behaviour of instant hot chocolate beverage: part 1. Optimization of the effect of different starches and gums. Food Biophys 6(4):512–518. https://doi.org/10.1007/s11483-011-9233-0

39. Duncan JM (1993) Limitations of conventional analysis of consolidation settlement. J Geotech Eng 119(9):1333–1359. https://doi.org/10.1061/(ASCE)0733-9410(1993)119:9(1333)

40. Eires R, Camões A, Jalali S (2015) Ancient materials and techniques to improve the earthen building durability. Key Eng Mater 634:357–366. https://doi.org/10.4028/www.scientific.net/KEM.634.357

41. Fam M, Santhamarian JC (1997) A study of consolidation using mechanical and electromagnetic waves. Géotechnique 47(2):203–219. https://doi.org/10.1680/geot.1997.47.2.203

42. Faris IH, Melchor J, Callejas A, Torres J, Rus G (2020) Viscoelastic biomarkers of Ex Vivo Liver Samples via torsional wave elastography. Diagnostics. https://doi.org/10.3390/diagnostics10020111

43. Fatehi H, Abtahi SM, Hashemolhosseini H, Hejazi SM (2018) A novel study on using protein based biopolymers in soil strengthening. Constr Build Mater 167:813–821. https://doi.org/10.1016/j.conbuildmat.2018.02.028

44. Feng S-J, Lu S-F, Shi Z-M, Shui W-H (2014) Densification of loosely deposited soft soils using the combined consolidation method. Eng Geol 181:169–179. https://doi.org/10.1016/j.enggeo.2014.07.010

45. Gingine V, Cardoso R (2017) Secondary consolidation of a consolidated kaolin slurry during electrokinetic treatment. Eng Geol 220:31–42. https://doi.org/10.1016/j.enggeo.2017.01.024

46. Gregory J, Barany S (2011) Adsorption and flocculation by polymers and polymer mixtures. Adv Colloid Interface 169(1):1–12. https://doi.org/10.1016/j.cis.2011.06.004

47. Gupta V, Hampton MA, Stokes JR, Nguyen AV, Miller JD (2011) Particle interactions in kaolinite suspensions and corresponding aggregate structures. J Colloid Interface Sci 359(1):95–103. https://doi.org/10.1016/j.jcis.2011.03.043

48. Ham S-M, Chang I, Noh D-H, Kwon T-H, Muhunthan B (2018) Improvement of surface erosion resistance of sand by microbial biopolymer formation. J Geotech Geoenviron 144(7):06018004. https://doi.org/10.1061/(ASCE)GT.1943-5606.0001900

49. Hataf N, Ghadir P, Ranjbar N (2018) Investigation of soil stabilization using chitosan biopolymer. J Clean Prod 170:1493–1500. https://doi.org/10.1016/j.jclepro.2017.09.256

50. Horpibulsuk S, Shibuya S, Fuenkajorn K, Katkan W (2007) Assessment of engineering properties of Bangkok clay. Can Geotech J 44(2):173–187. https://doi.org/10.1139/t06-101

51. Im J, Tran ATP, Chang I, Cho G-C (2017) Dynamic properties of gel-type biopolymer-treated sands evaluated by Resonant Column (RC) tests. Geomech Eng 12(5):815–830. https://doi.org/10.12989/gae.2017.12.5.815

52. Indraratna B, Sathananthan I, Rujikiatkamjorn C, Balasubramaniam AS (2005) Analytical and numerical modeling of soft soil stabilized by prefabricated vertical drains incorporating vacuum preloading. Int J Geomech 5(2):114–124. https://doi.org/10.1061/(ASCE)1532-3641(2005)5:2(114)

53. Jayasekera S (2015) Electrokinetics to modify strength characteristics of soft clayey soils: a laboratory based investigation.

Electrochim Acta 181:39–47. https://doi.org/10.1016/j.electacta.2015.06.064

54. Joga JR, Varaprasad BJS (2019) Sustainable improvement of expansive clays using xanthan gum as a biopolymer. Civ Eng J 5(9):1893–1903. https://doi.org/10.28991/cej-2019-03091380

55. Kang X, Bate B (2016) Shear wave velocity and its anisotropy of polymer modified high-volume class-F Fly-kaolinite mixtures. J Geotech Geoenviron 142(12):04016068. https://doi.org/10.1061/(ASCE)GT.1943-5606.0001562

56. Kang X, Cao J, Bate B (2019) Large-strain strength of polymer-modified kaolinite and fly ash–kaolinite mixtures. J Geotech Geoenviron 145(2):04018106. https://doi.org/10.1061/(ASCE)GT.1943-5606.0002008

57. Kang X, Cao J, Bate B (2020) Shear wave velocity anisotropy of salt- and polymer-amended kaolinite. Acta Geotech. https://doi.org/10.1007/s11440-020-00974-0

58. Karol RH (2003) Chemical grouting and soil stabilization. Marcel Dekker Inc, New York

59. Karunaratne GP, Chew SH, Lee SL, Sinha AN (2001) Bentonite: kaolinite clay liner. Geosynth Int 8(2):113–133. https://doi.org/10.1680/gein.8.0189

60. Katzbauer B (1998) Properties and applications of xanthan gum. Polym Degrad Stabil 59(1):81–84. https://doi.org/10.1016/S0141-3910(97)00180-8

61. Khatami H, O'Kelly B (2012) Improving mechanical properties of sand using biopolymers. J Geotech Geoenviron 139(8):1402–1406. https://doi.org/10.1061/(ASCE)GT.1943-5606.0000861

62. Kim A-R, Chang I, Cho G-C, Shim S-H (2018) Strength and dynamic properties of cement-mixed Korean marine clays. KSCE J Civ Eng 22(4):1150–1161. https://doi.org/10.1007/s12205-017-1686-3

63. Koerner RM, Fowler J, Lawrence CA (1986) Soft soil stabilization study for Wilmington Harbor South dredge material disposal area. Army engineer waterways experiment station vicksburgs MS geotechnical lab

64. Koerner RM, Hwu B-L, Wayne MH (1987) Soft soil stabilization designs using geosynthetics. Geotext Geomembr 6(1):33–51. https://doi.org/10.1016/0266-1144(87)90056-2

65. Komine H, Watanabe Y (2010) The past, present and future of the geo-environment in Japan. Soils Found 50(6):977–982. https://doi.org/10.3208/sandf.50.977

66. Koumoto T, Houlsby GT (2001) Theory and practice of the fall cone test. Géotechnique 51(8):701–712. https://doi.org/10.1680/geot.2001.51.8.701

67. Kwon Y-M, Chang I, Lee M, Cho G-C (2019) Geotechnical engineering behaviors of biopolymer-treated soft marine soil. Geomech Eng 17(5):453–464. https://doi.org/10.12989/GAE.2019.17.5.453

68. Kwon Y-M, Cho G-C, Chung M-K, Chang I (2021) Surface erosion behavior of biopolymer-treated river sand. Geomech Eng 25(1):49–58. https://doi.org/10.12989/gae.2021.25.1.049

69. Kwon Y-M, Ham S-M, Kwon T-H, Cho G-C, Chang I (2020) Surface-erosion behaviour of biopolymer-treated soils assessed by EFA. Geotech Lett 10(2):1–7. https://doi.org/10.1680/jgele.19.00106

70. Kwon Y-M, Im J, Chang I, Cho G-C (2017) ε-polylysine biopolymer for coagulation of clay suspensions. Geomech Eng 12(5):753–770. https://doi.org/10.12989/gae.2017.12.5.753

71. Latifi N, Horpibulsuk S, Meehan CL, Majid MZA, Tahir MM, Mohamad ET (2017) Improvement of problematic soils with biopolymer—an environmentally friendly soil stabilizer. J Mater Civ Eng 29(2):04016204. https://doi.org/10.1061/(ASCE)MT.1943-5533.0001706

72. Latifi N, Rashid ASA, Marto A, Tahir MM (2016) Effect of magnesium chloride solution on the physico-chemical

characteristics of tropical peat. Environ Earth Sci 75(3):220. https://doi.org/10.1007/s12665-015-4788-6

73. Lee JS, Santamarina JC (2005) Bender elements: performance and signal interpretation. J Geotech Geoenviron 131(9):1063–1070. https://doi.org/10.1061/(ASCE)1090-0241(2005)131:9(1063)

74. Li X, Li Q, Yang S, Yang G (2019) Swelling of clay minerals: dual characteristics of K^+ ions and exploration of critical influencing factors. Phys Chem Chem Phys 21(4):1963–1971. https://doi.org/10.1039/c8cp07567k

75. Luo H-L, Hsiao D-H, Lin D-F, Lin C-K (2012) Cohesive soil stabilized using sewage sludge Ash/cement and nano aluminum oxide. Int J Transp Sci Technol 1(1):83–99. https://doi.org/10.1260/2046-0430.1.1.83

76. Martin G, Yen T, Karimi S (1996) Application of biopolymer technology in silty soil matrices to form impervious barriers. In: 7th Australia New Zealand Conference on geomechanics: geomechanics in a changing world: conference proceedings, p 814

77. Martinez-Nistal A, Veniale F, Setti M, Cotecchia F (1999) A scanning electron microscopy image processing method for quantifying fabric orientation of clay geomaterials. Appl Clay Sci 14(4):235–243. https://doi.org/10.1016/S0169-1317(98)00055-6

78. Md Zahri A, Zainorabidin A (2019) An overview of traditional and non traditional stabilizer for soft soil. IOP Conf Ser Mater Sci Eng 527(1):012015. https://doi.org/10.1088/1757-899x/527/1/012015

79. Menon ES (1978) Pipeline planning and construction field manual. Gulf Professional Publishing

80. Mitchell JK, Soga K (2005) Fundamentals of soil behavior. Wiley, Hoboken

81. Ni J, Hao G-L, Chen J-Q, Ma L, Geng X-Y (2021) The optimisation analysis of sand-clay mixtures stabilised with xanthan gum biopolymers. Sustainability 13(7):3732. https://doi.org/10.3390/su13073732

82. Ni J, Li S-S, Ma L, Geng X-Y (2020) Performance of soils enhanced with eco-friendly biopolymers in unconfined compression strength tests and fatigue loading tests. Constr Build Mater 263:120039. https://doi.org/10.1016/j.conbuildmat.2020.120039

83. Noh D-H, Ajo-Franklin JB, Kwon T-H, Muhunthan B (2016) P and S wave responses of bacterial biopolymer formation in unconsolidated porous media. J Geophys Res Biogeosci 121(4):1158–1177. https://doi.org/10.1002/2015jg003118

84. Nugent RA, Zhang G, Gambrell RP (2011) The effect of exopolymers on the compressibility of clays. Geo-Frontiers 2011:3935–3944. https://doi.org/10.1061/41165(397)402

85. Nugent RA, Zhang G, Gambrell RP (2009) Effect of exopolymers on the liquid limit of clays and its engineering implications. Transp Res Record 2101(1):34–43. https://doi.org/10.3141/2101-05

86. Nugent RA, Zhang G, Gambrell RP (2010) The effects of exopolymers on the erosional resistance of cohesive sediments. In: International conference on scour and erosion, pp 162–171. https://doi.org/10.1061/41147(392)15

87. Orts WJ, Sojka RE, Glenn GM (2000) Biopolymer additives to reduce erosion-induced soil losses during irrigation. Ind Crop Prod 11(1):19–29. https://doi.org/10.1016/S0926-6690(99)00030-8

88. Phetchuay C, Horpibulsuk S, Arulrajah A, Suksiripattanapong C, Udomchai A (2016) Strength development in soft marine clay stabilized by fly ash and calcium carbide residue based geopolymer. Appl Clay Sci 127–128:134–142. https://doi.org/10.1016/j.clay.2016.04.005

89. Pooja D, Panyaram S, Kulhari H, Rachamalla SS, Sistla R (2014) Xanthan gum stabilized gold nanoparticles: characterization, biocompatibility, stability and cytotoxicity. Carbohyd Polym 110:1–9. https://doi.org/10.1016/j.carbpol.2014.03.041

90. Reddy JJ, Varaprasad BJS (2021) Long-term and durability properties of xanthan gum treated dispersive soils—an eco-friendly material. Mater Today Proc 44:309–314. https://doi.org/10.1016/j.matpr.2020.09.472

91. Robinson RG, Allam MM (1998) Effect of clay mineralogy on coefficient of consolidation. Clay Clay Miner 46(5):596–600. https://doi.org/10.1346/CCMN.1998.0460514

92. Sachan A, Penumadu D (2007) Effect of microfabric on shear behavior of kaolin clay. J Geotech Geoenviron 133(3):306–318. https://doi.org/10.1061/(ASCE)1090-0241(2007)133:3(306)

93. Santamarina JC, Klein KA, Wang YH, Prencke E (2002) Specific surface: determination and relevance. Can Geotech J 39(1):233–241. https://doi.org/10.1139/t01-077

94. Seo S, Lee M, Im J, Kwon Y-M, Chung M-K, Cho G-C, Chang I (2021) Site application of biopolymer-based soil treatment (BPST) for slope surface protection: in-situ wet-spraying method and strengthening effect verification. Constr Build Mater 307:124983. https://doi.org/10.1016/j.conbuildmat.2021.124983

95. Shalviri A, Liu Q, Abdekhodaie MJ, Wu XY (2010) Novel modified starch–xanthan gum hydrogels for controlled drug delivery: synthesis and characterization. Carbohyd Polym 79(4):898–907. https://doi.org/10.1016/j.carbpol.2009.10.016

96. Sherwood PT (1993) Soil stabilization with cement and lime. HMSO, London

97. Singh SP, Das R (2020) Geo-engineering properties of expansive soil treated with xanthan gum biopolymer. Geomech Geoeng 15(2):107–122. https://doi.org/10.1080/17486025.2019.1632495

98. Soldo A, Miletić M, Auad ML (2020) Biopolymers as a sustainable solution for the enhancement of soil mechanical properties. Sci Rep 10(1):267. https://doi.org/10.1038/s41598-019-57135-x

99. Sujatha ER, Atchaya S, Sivasaran A, Keerdthe RS (2020) Enhancing the geotechnical properties of soil using xanthan gum—an eco-friendly alternative to traditional stabilizers. Bull Eng Geol Environ. https://doi.org/10.1007/s10064-020-02010-7

100. Sujatha ER, Saisree S (2019) Geotechnical behaviour of guar gum-treated soil. Soils Found 59(6):2155–2166. https://doi.org/10.1016/j.sandf.2019.11.012

101. Da S, Sun W, Fang L (2014) Swelling characteristics of Gaomiaozi bentonite and its prediction. J Rock Mech Geotech Eng 6(2):113–118. https://doi.org/10.1016/j.jrmge.2014.01.001

102. Da S, Zhang J, Zhang J, Zhang L (2013) Swelling characteristics of GMZ bentonite and its mixtures with sand. Appl Clay Sci 83–84:224–230. https://doi.org/10.1016/j.clay.2013.08.042

103. Talukdar MM, Kinget R (1995) Swelling and drug release behaviour of xanthan gum matrix tablets. Int J Pharm 120(1):63–72. https://doi.org/10.1016/0378-5173(94)00410-7

104. Tan X, Hu L, Reed A, Furukawa Y, Zhang G (2014) Flocculation and particle size analysis of expansive clay sediments affected by biological, chemical, and hydrodynamic factors. Ocean Dyn 64(1):143–157. https://doi.org/10.1007/s10236-013-0664-7

105. Taylor DW (1948) Fundamentals of soil mechanics. Wiley, New York

106. Thakur V, Singh D (2005) Rapid determination of swelling pressure of clay minerals. J Test Eval 33(4):239–245. https://doi.org/10.1520/JTE11866

107. Theng BKG (1982) Clay-polymer interactions: Summary and perspectives. Clay Clay Miner 30(1):1–10. https://doi.org/10.1346/CCMN.1982.0300101

108. Theng BKG (2012) Formation and properties of clay-polymer complexes. Elsevier, Amsterdam

109. Tombácz E, Szekeres M (2006) Surface charge heterogeneity of kaolinite in aqueous suspension in comparison with montmorillonite. Appl Clay Sci 34(1):105–124. https://doi.org/10.1016/j.clay.2006.05.009

110. US Environmental Protection Agency (1998) Evaluation of subsurface engineered barriers at waste sites. United States Environmental Protection Agency, Washington

111. Vydehi Kopparthi V, Moghal Arif Ali B (2022) Effect of biopolymeric stabilization on the strength and compressibility characteristics of cohesive soil. J Mater Civil Eng 34(2):04021428. https://doi.org/10.1061/(ASCE)MT.1943-5533.0004068

112. Vydehi KV, Moghal AAB, Basha BM (2022) Reliability-based design optimization of biopolymer-amended soil as an alternative landfill liner material. J Hazard Toxic Radioact Waste 26(3):04022011. https://doi.org/10.1061/(ASCE)HZ.2153-5515.0000697

113. Wang YH, Xu D (2007) Dual porosity and secondary consolidation. J Geotech Geoenviron 133(7):793–801. https://doi.org/10.1061/(ASCE)1090-0241(2007)133:7(793)

114. World Health Organization (2016) Evaluation of certain food additives: eighty-second report of the Joint FAO/WHO Expert Committee on Food Additives. World Health Organization, Geneva

115. Yeo S-S, Shackelford CD, Evans JC (2005) Consolidation and hydraulic conductivity of nine model soil-bentonite backfills. J Geotech Geoenviron 131(10):1189–1198. https://doi.org/10.1061/(ASCE)1090-0241(2005)131:10(1189)

116. Yoon GL, Kim BT (2006) Regression analysis of compression index for Kwangyang marine clay. KSCE J Civ Eng 10(6):415–418. https://doi.org/10.1007/BF02823980

117. Zhang G, Yin H, Lei Z, Reed AH, Furukawa Y (2013) Effects of exopolymers on particle size distributions of suspended cohesive sediments. J Geophys Res Oceans 118(7):3473–3489. https://doi.org/10.1002/jgrc.20263